MAGNETOHYDRODYNAMICS OF INSULATING SPHERES

J.W. Haverkort[1], *T.W.J. Peeters*[2]

[1] *Delft University of Technology, Applied Physics,*
Lorentzweg 1, 2628 CJ Delft, The Netherlands
e-Mail: J.W.Haverkort@cwi.nl
[2] *Corus Research Development and Technology,*
P.O. Box 10.000 1970 CA IJmuiden, The Netherlands

The effect of electric and magnetic fields on a conducting fluid surrounding an insulating object plays a role in various industrial, biomedical and micro-fluidic applications. Computational simulations of the magnetohydrodynamic flow around an insulating sphere, with crossed magnetic and electric fields perpendicular to the main flow, are performed for $Rm \ll 1$ in the ranges $0.1 \leq Re \leq 100$, $1 \leq Ha \leq 20$ and $10^{-2} \leq N \leq 10^{3}$. Careful examination of this fundamental three-dimensional flow reveals a rich physical structure with surface charge on the sphere neighbouring volume charge of opposite sign. Hartmann layers, circulating current and asymmetric velocity and current profiles appear as a result of the applied magnetic and electric field. A parametric study on the magnetic field's influence on the drag coefficient is performed computationally. The obtained results bridge a gap between various analytical solutions of limiting cases and show good correspondence to earlier work. Correlations for the drag coefficient are proposed that can be valuable for the description of insulating inclusions in various flow applications with magnetic fields.

1. Introduction. Magnetic fields are frequently used in industrial applications to control the flow of conducting fluids. In the steel industry, for example, large electromagnets are used to dampen unwanted fluid motion at free surfaces, control the degree of turbulence, stir the liquid [1], and influence the solidification process [2]. Due to the finite conductivity of biological fluids like blood, magnetohydrodynamics also plays a role in biomedical applications like Magnetic Drug Targeting (MDT) and (immuno)magnetic cell separation [3]. In recent years, interest has arisen in using magnetohydrodynamics in micro-fluidic devices to stir, cool and pump fluids for, e.g., chromatography or the replication of DNA [4]. In many of these applications the conducting fluid also contains insulating inclusions or bubbles. Although insulating objects do not experience a magnetic force directly, there are some effects associated with the fact that the liquid surrounding the insulating object does. Best known is the electromagnetic Archimedes force, also known as the electromagnetic buoyancy force or electromagnetophoretic force [5]. This force acts on an insulating object as a reaction to the magnetic force density $\mathbf{J} \times \mathbf{B}$ on the surrounding conducting fluid, in a similar manner as its gravitational counterpart. The electromagnetic Archimedes force is used in separation techniques, for example, to purify liquid metals from less conductive inclusions [6]. Another noteworthy effect is an observed increase in the drag force on insulating objects in the presence of a magnetic field. The fundamental problem of an insulating sphere in a flowing conducting medium has been investigated analytically for Rm, Re, $Ha \ll 1$ for a magnetic field parallel to the flow [7] and was later extended to include an arbitrary field orientation [8]. The results of this magnetohydrodynamic analogue of the Stokes flow show a fractional increase in the drag coefficient proportional to Ha. An increased drag was also found in the

analytical solution of the magnetohydrodynamic potential flow around a sphere [9]. In the limit Re $\gg$ 1 and N $\ll$ 1 the increase in drag coefficient was found to be proportional to N = Ha^2/Re. Actual measurements performed in the 1960's [10, 11] indicated a dependence on $\sqrt{N}$, more or less in accordance with the theory for Ha$^2 \gg$ Re $\gg$ 1 [12, 13]. These various regimes hint to a wealth of interesting physics and show that the drag curve, intensively studied for ordinary flow around spheres, in magnetohydrodynamics can no longer be described in terms of a single dimensionless number. In the presence of a magnetic field with a specific orientation, the drag curve becomes a "drag surface" as a function of both Re and Ha or N. Recently, numerical simulations have been added to these investigations. Refs. [14, 15] deal with the axially symmetric case of a magnetic field aligned with the flow. Although a magnetic field orientation perpendicular to the flow makes analysis more complex due to the inherent three-dimensionality, it is the more relevant case from the application point of view. Magnetic fields perpendicular to the flow can be used to brake the flow, generate electricity or work as an electromagnetic pump. This work aims to add to our understanding and knowledge of this important basic flow configuration and give insight into the mechanisms behind the magnetohydrodynamic flow around insulating objects.

2. Theoretical considerations. The dimensionless numbers in this work are related to quantities pertaining to the sphere, in particular, the characteristic length scale is taken to be the sphere diameter D. The Hartmann number, Reynolds number and the interaction parameter (or Stuart number) are then defined as Ha $\equiv B_0 D \sqrt{\sigma/\rho\nu}$, Re $\equiv u_0 D/\nu$ and N $\equiv$ Ha^2/Re $= \sigma B_0^2 D/\rho u_0$, with B_0 being the applied magnetic field, $u_0 = |\mathbf{u}_0|$ the magnitude of the main flow (far-field) velocity and ρ, ν and σ the fluid mass density, kinematic viscosity and electric conductivity, respectively. This paper deals with situations, in which the the magnetic Reynolds number Rm $\equiv \mu_0 \sigma u_0 D \ll$ 1 so that the magnetic field induced by the electric currents in the fluid can be neglected. The electric current density $\mathbf{J}$ is assumed to be proportional to the electric field in a frame moving with the fluid velocity $\mathbf{u}$, as stated by the Ohm's law for moving media:

$$\mathbf{J} = \sigma \left(\mathbf{E} + \mathbf{u} \times \mathbf{B} \right). \tag{1}$$

In a confined domain, an electric field perpendicular to both the main flow velocity $\mathbf{u}_0$ and an applied magnetic field $\mathbf{B}_0$ naturally arises due to the accumulation of charge at the domain boundaries. When the walls of the domain are electrically insulating and the size of the domain is large compared to the thickness of the Hartmann layers, these charges create an electric field $\mathbf{E} \approx -\mathbf{u}_0 \times \mathbf{B}_0$ almost entirely cancelling the formation of electric current. This situation is mathematically identical to the situation, in which one moves relative to a still conducting fluid in the presence of a constant magnetic field. Moving with a non-relativistic velocity $\mathbf{u}_0$, the electromagnetic fields transform so that one observes an unmodified magnetic field and an additional electric field $\mathbf{E} = -\mathbf{u}_0 \times \mathbf{B}_0$. In magnetohydrodynamics, the fluid conductivity is assumed to be high so that under the influence of electric forces alone the excess charge can only reside at the domain boundaries. However, magnetic forces can keep a small net volume charge in place within the fluid [1]. In steady state $\mathbf{J}$ is divergence-free so that from Eq. 1 inside the flow

$$\mathrm{div}\mathbf{E} = -\mathbf{B} \cdot \mathrm{rot}\,\mathbf{u}, \tag{2}$$

where use is made of the mathematical identity div($\mathbf{u} \times \mathbf{B}$) = $\mathbf{B} \cdot$ rot $\mathbf{u} - \mathbf{u} \cdot$ rot $\mathbf{B}$ and the fact that for Rm $\ll$ 1 the last term can be neglected. Introducing the

fluid vorticity $\boldsymbol{\omega} \equiv \operatorname{rot} \mathbf{u}$ and using the Gauss's law $\operatorname{div}\mathbf{E} = \rho_e/\epsilon_0$, with ρ_e being the volumetric charge density, Eq. 2 becomes

$$\rho_e = -\epsilon_0 \boldsymbol{\omega} \cdot \mathbf{B}. \tag{3}$$

Whenever the vorticity is to some degree aligned with the magnetic field, volume charges will thus be present. When a magnetic field is applied parallel to the flow around a sphere, for not too high Reynolds numbers, the flow is axially symmetric so that the vorticity is everywhere perpendicular to the magnetic field. For this field orientation used in the simulations of Refs. [14, 15], the volume charge ρ_e, therefore, vanishes. The drag force on the sphere is found by integrating the hydrodynamic stress-tensor $\mathbb{T} = p\mathbb{I} + \rho\nu(\operatorname{grad}\mathbf{u} + (\operatorname{grad}\mathbf{u})^{\mathrm{T}})$ for an incompressible Newtonian fluid over the surface of the sphere

$$\mathbf{F}_D = \int_V \operatorname{div}\mathbb{T}\mathrm{d}V = \int_{\partial V} p\mathrm{d}\mathbf{S} + \int_{\partial V} \rho\nu(\operatorname{grad}\mathbf{u} + (\operatorname{grad}\mathbf{u})^{\mathrm{T}}) \cdot \mathrm{d}\mathbf{S}.$$

The drag force changes in the presence of a magnetic field due to the modifications the magnetic force induces in the velocity and pressure. For low interaction parameters N, the flow is influenced only slightly by the magnetic field. The additional "electromagnetic drag force" F_{Dem} due to the magnetic field can then be written in terms of Joule dissipation as an integral over the fluid volume V

$$F_{\mathrm{Dem}} = \frac{1}{u_0} \int_V \frac{J^2}{\sigma}\mathrm{d}V.$$

The "electromagnetic drag coefficient" $C_{\mathrm{Dem}} \equiv F_{\mathrm{Dem}}/\frac{1}{2}\rho(\frac{1}{4}\pi D^2)u_0^2$ attributable to this added electromagnetic drag in terms of the nondimensionalized quantities $J' \equiv J/\sigma u_0 B_0$ and $V' \equiv V/D^3$ becomes

$$\begin{aligned}
C_{\mathrm{Dem}} &\equiv & \frac{F_{\mathrm{Dem}}}{\frac{1}{2}\rho(\frac{1}{4}\pi D^2)u_0^2} = \frac{8}{\pi\rho D^2 u_0^3} \int_V \frac{J^2}{\sigma}\mathrm{d}V \\
&= & \frac{8}{\pi}\frac{\sigma B^2 D}{\rho u_0} \int_V J'^2\mathrm{d}V' = \frac{8}{\pi}\mathrm{N} \int_V J'^2\mathrm{d}V'
\end{aligned}$$

When this last integral is independent of N, the drag coefficient is proportional to N. This is in accordance with the result of Ref. [9] for a magnetic field perpendicular to the flow:

$$C_{\mathrm{Dem}} = \frac{3}{10}\mathrm{N} \qquad \mathrm{N} \ll 1, \mathrm{Re} \gg 1. \tag{4}$$

In the asymptotic theory of Ref. [12], the size of the insulating object is assumed to be of the same order of magnitude as the size of the duct, in which it is placed, leading to a magnetic field perpendicular to the flow to [13]

$$C_{\mathrm{Dem}} = \frac{8}{\sqrt{\mathrm{Re}}}\sqrt{\mathrm{N}} \qquad \mathrm{N}, \mathrm{Re} \gg 1. \tag{5}$$

This expression is in reasonable correspondence with the experimental results, which have been fitted by [10]

$$C_{\mathrm{Dem}} \approx 0.7 C_{\mathrm{D0}}\sqrt{\mathrm{N}},$$

with C_{D0} being the drag coefficient in the absence of a magnetic field. For completeness, we cite the result for the Stokes flow in the presence of a magnetic field perpendicular to the main flow [8], for which $C_{\mathrm{D0}} = 24/\mathrm{Re}$

$$C_{\mathrm{Dem}} = \frac{9}{16}C_{\mathrm{D0}}\mathrm{Ha} = \frac{27}{2}\frac{\mathrm{Ha}}{\mathrm{Re}} = \frac{27}{2\sqrt{\mathrm{Re}}}\sqrt{\mathrm{N}} \qquad \mathrm{Re}, \mathrm{Ha} \ll 1. \tag{6}$$
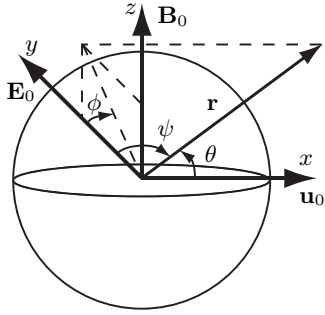
Fig. 1. A schematic overview of the coordinates used and the directions of the main flow velocity $\mathbf{u}_0$, the applied magnetic $\mathbf{B}_0$ and electric $\mathbf{E}_0$ fields.

3. Methods. The performed simulations concerned the steady state flow of an incompressible Newtonian fluid and have been performed by CFX 11 Computational Fluid Dynamics software by Ansys, Inc. This linear solver solves the Navier–Stokes equations extended by a magnetic force density $\mathbf{J} \times \mathbf{B}$. The current density $\mathbf{J}$ is assumed to satisfy Eq. 1 and in steady state is divergence-free, so that with $\mathbf{E} = -\operatorname{grad}\Phi$

$$\nabla^2 \Phi = \operatorname{div}\left(\mathbf{u} \times \mathbf{B}\right).$$

This Poisson equation for the electric potential Φ is solved self-consistently with the Navier–Stokes equation. The magnetohydrodynamic capabilities of the solver have been validated by comparing with analytical expressions of Ref. [16]. The main simulations used approximately 400,000 elements, in which care was taken to include sufficient cells within boundary layers. The parametric drag studies were performed on a coarser mesh of approximately 100,000 elements. The influence of the sphere on the flow near the domain boundaries was found to become negligible for a computational domain $10D \times 15D \times 45D$ in size, which was used for the simulations. In all simulations the material properties used were approximately those of liquid steel: $\rho = 7 \cdot 10^3$ kgm^{-3}, $\nu = 10^{-6}$ m^{2}s^{-1} and $\sigma = 7 \cdot 10^5$ Ω^{-1}. The values used for the main flow velocity $u_0 = \mathcal{O}(10^{-4}\text{--}10^{-1}$ ms$^{-1})$, magnetic field $B_0 = \mathcal{O}(10^{-1}$ T$)$ and sphere diameter $D = \mathcal{O}(10^{-3}$ m$)$ are representative of those of industrial applications.

4. Results. Computational simulations have been performed for the magnetohydrodynamic flow around an insulating sphere. A large rectangular computational domain with free-slip sidewalls was used with a constant inlet and outlet velocity $\mathbf{u}_0$. A magnetic field $\mathbf{B}_0$ was applied perpendicular to the flow as shown in Fig. 1. An electric field $\mathbf{E}_0 = -\mathbf{u}_0 \times \mathbf{B}_0$ was applied to prevent the formation of electric currents far away from the sphere. As discussed in Section 2, this situation corresponds to either a sphere with a slip-velocity $\mathbf{u}_0$ in a large channel flow, or a sphere moving with a velocity $\mathbf{u}_0$ through a still fluid in the presence of a magnetic field.

As a base case, in Section 4.1, the results are discussed for $u_0 = 0.01$ m/s, $D = 1$ mm and $B_0 = 0.2$ T so that Re $= 10$, Ha $= 2$ and N $=$ Ha^2/Re $= 0.4$. In this case, the influence of the magnetic force is significant, but many of the phenomena from ordinary fluid mechanics dominate. In Section 4.2 several other parameter ranges are investigated. Finally, in Section 4.3, a parametrization study is performed for the electromagnetic drag on the sphere.

4.1. Base case. The electric current density $\mathbf{J}$ is governed by the balance between $\mathbf{E}$ and $\mathbf{u} \times \mathbf{B}_0$ of Eq. 1:

$$\mathbf{J} = \sigma\left(\mathbf{E} + \mathbf{u} \times \mathbf{B}_0\right)$$

and is shown in Fig. 2 in the vicinity of the sphere. In the Hartmann layer at the top and bottom of the sphere (positive and negative z, respectively), the electric current is oriented in the y-direction of the electric field $\mathbf{E}_0$. Further away from the sphere, the fluid velocity increases slightly above the main flow velocity $\mathbf{u}_0$ so that the direction of the current is reversed. Consequently, very close to the top and bottom of the sphere the Lorentz force $\mathbf{J} \times \mathbf{B}_0$ accelerates the fluid, while it decelerates the fluid a little further away. On the sides of the sphere, the current is in the y-direction up to a much larger distance from the sphere compared to that near the top and bottom. The associated Lorentz force on the sides of the sphere accelerates the fluid to a value above the main flow velocity $u_0 = 0.01$ m/s,
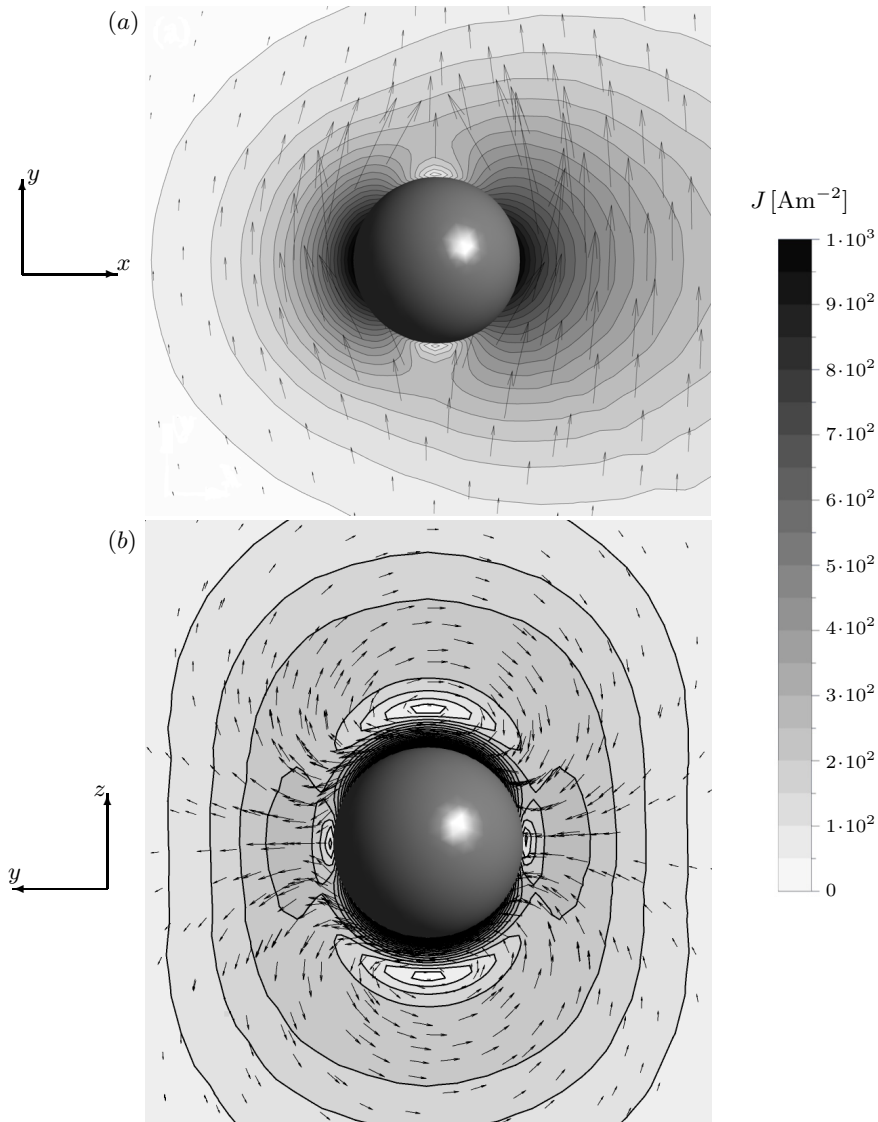

Fig. 2.   Contours and vectors of the electric current density $\mathbf{J}$ in (*a*) the xy-plane perpendicular to the magnetic field and in (*b*) the yz-plane perpendicular to the main flow velocity. The area, over which the electric current is oriented in the y-direction is much larger behind the sphere than in front of the sphere, reflecting the asymmetry expected for Re = 10 (and Ha = 2).
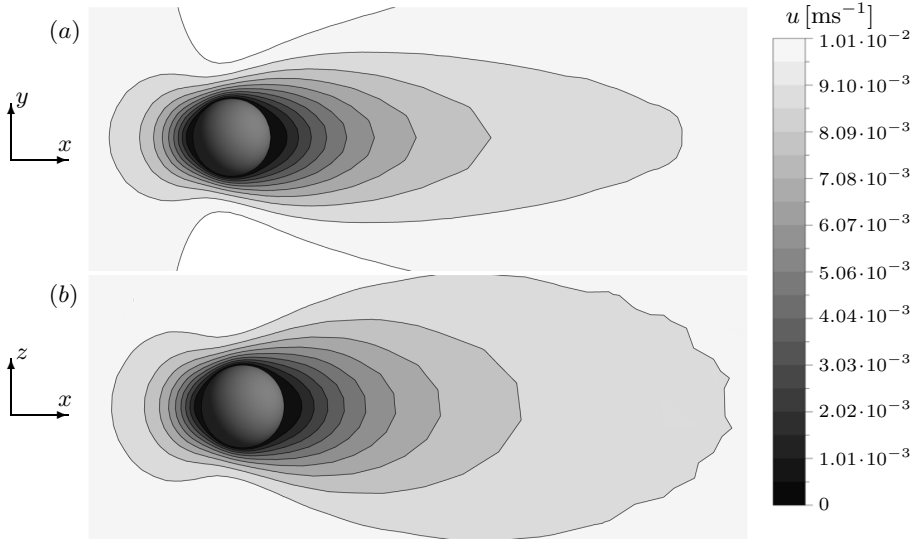
Fig. 3. The velocity wake in (*a*) an *xy*-plane perpendicular and (*b*) an *xz*-plane parallel to the magnetic field. A distinct asymmetry, with a preference for a velocity spread along the field lines, can be seen behind the sphere. A characteristic dent in the velocity contours can be observed near the sides of the sphere. This is due to the electric field the volume charges here add to $\mathbf{E}_0$, which increases the electric current in the *y*-direction and thereby increases the accelerating Lorentz force.

as can be clearly seen in Figs. 3*a* and 4*a*. Because the component of $\mathbf{u} \times \mathbf{B}_0$ in the negative *y*-direction in this region exceeds the magnitude of $\mathbf{E}_0$ in the positive *y*-direction, an additional electric field must be responsible for the orientation of the current in the positive *y*-direction. This additional electric field can indeed be observed from Fig. 5, which shows the radial electric field component E_r. The electric field in the *y*-direction near the sides of the sphere clearly exceeds the applied electric field $E_0 = u_0 B_0 = 0.02$ V/m. We then investigate the origin of this electric field.

Because no current can enter the insulating sphere, the radial electric field vanishes at the surface of the sphere as can indeed be observed from Fig. 5. From the Gauss's law div$\mathbf{E} = \rho/\epsilon_0$, the discontinuity in the electric field over the surface of the sphere can be related to the presence of a surface charge σ_s

$$E_{r,\text{out}} - E_{r,\text{in}} = \sigma_s/\epsilon_0. \tag{7}$$

This surface charge, negative for positive *y* and positive for negative *y*, is responsible for the cancellation of the radial electric field on the surface of the sphere by generating an electric field in the negative *y*-direction just outside the sphere. This surface charges, therefore, cannot be responsible for the observed additional electric field in the *positive y*-direction. At the sides of the sphere the vorticity is aligned with the magnetic field so that from Eq. 3 a volume charge density $\rho_e = -\boldsymbol{\omega} \cdot \mathbf{B}_0$ will be present as well. For positive *y*, the vorticity is in the negative *z*-direction, anti-parallel to the magnetic field, so that a positive volume charge arises. For negative *y*, the vorticity is in the positive *z*-direction, parallel to the magnetic field, so that a negative volume charge arises. The electric field generated by these volume charges is, some distance from the sides of the sphere, oriented in the positive *y*-direction and responsible for the observed additional electric field. These volume charges, kept in place by the magnetic force, thus play a crucial role in describing the electric current distribution and thereby the flow field around the
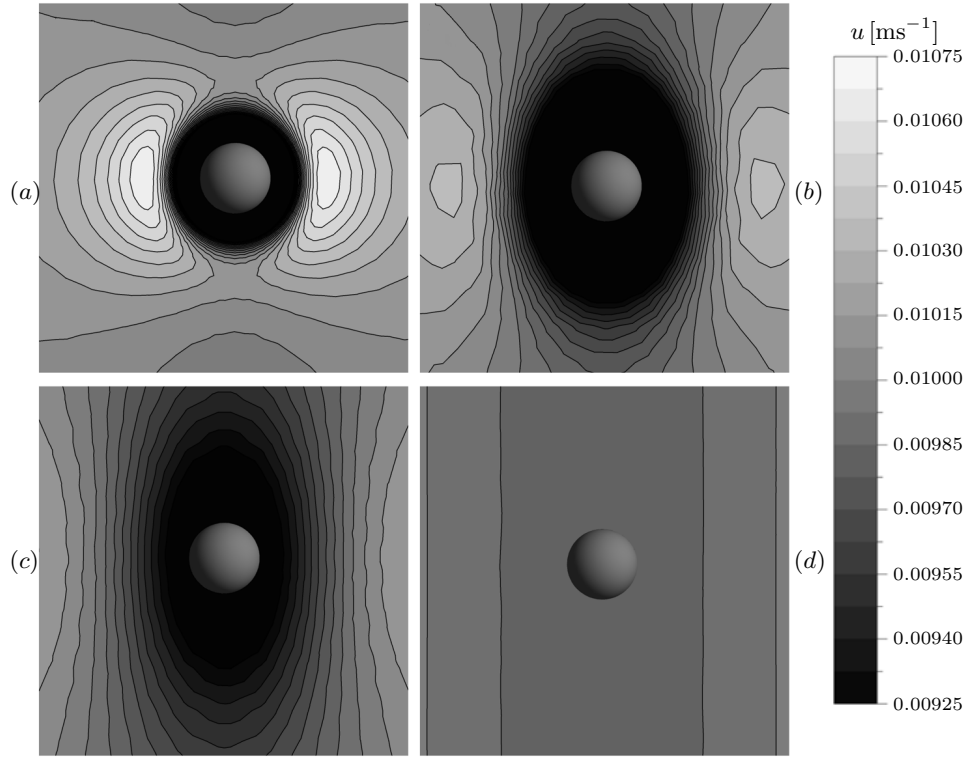
116

Fig. 4. The velocity in the yz-plane at $x = 0D$, $2D$, $5D$ and $30D$ behind the center of the sphere of diameter $D = 1$ mm (Re = 10, Ha = 2).
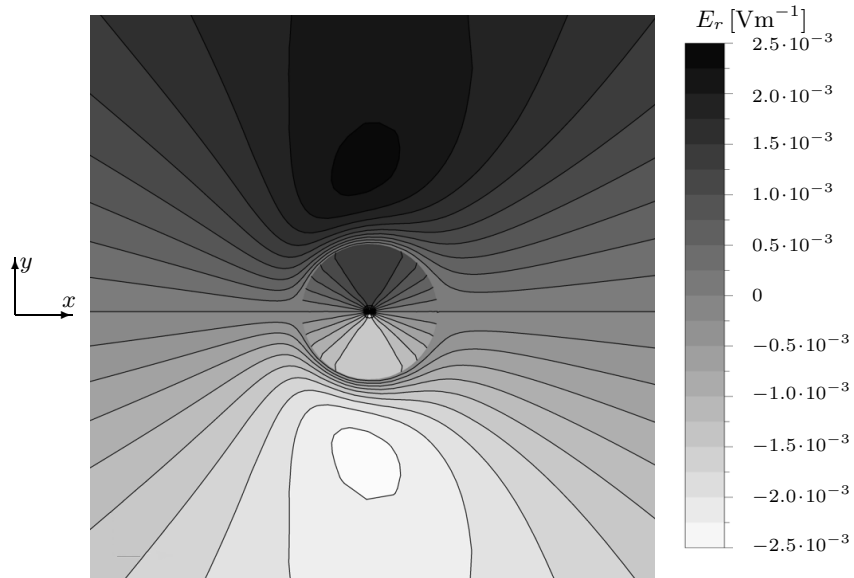

Fig. 5. The radial component E_r of the electric field in the xy-plane for Re = 10 and Ha = 2. Note that E_r vanishes at the boundary of the insulating sphere. The symmetry in the yz-plane is broken by the advection of volume charge close to the sphere.

117

sphere. The resulting volume charge density is shown in Fig. 6 and a schematic overview of the location of the electric charges is given in Fig. 7. An overview of the surface charge, volume charge and the electric field these charges generate is given in Fig. 8. When close to the sphere, the surface charge creates an electric field in the negative y-direction; further away from the sphere the volume charges change the direction of the electric field to the positive y-direction.
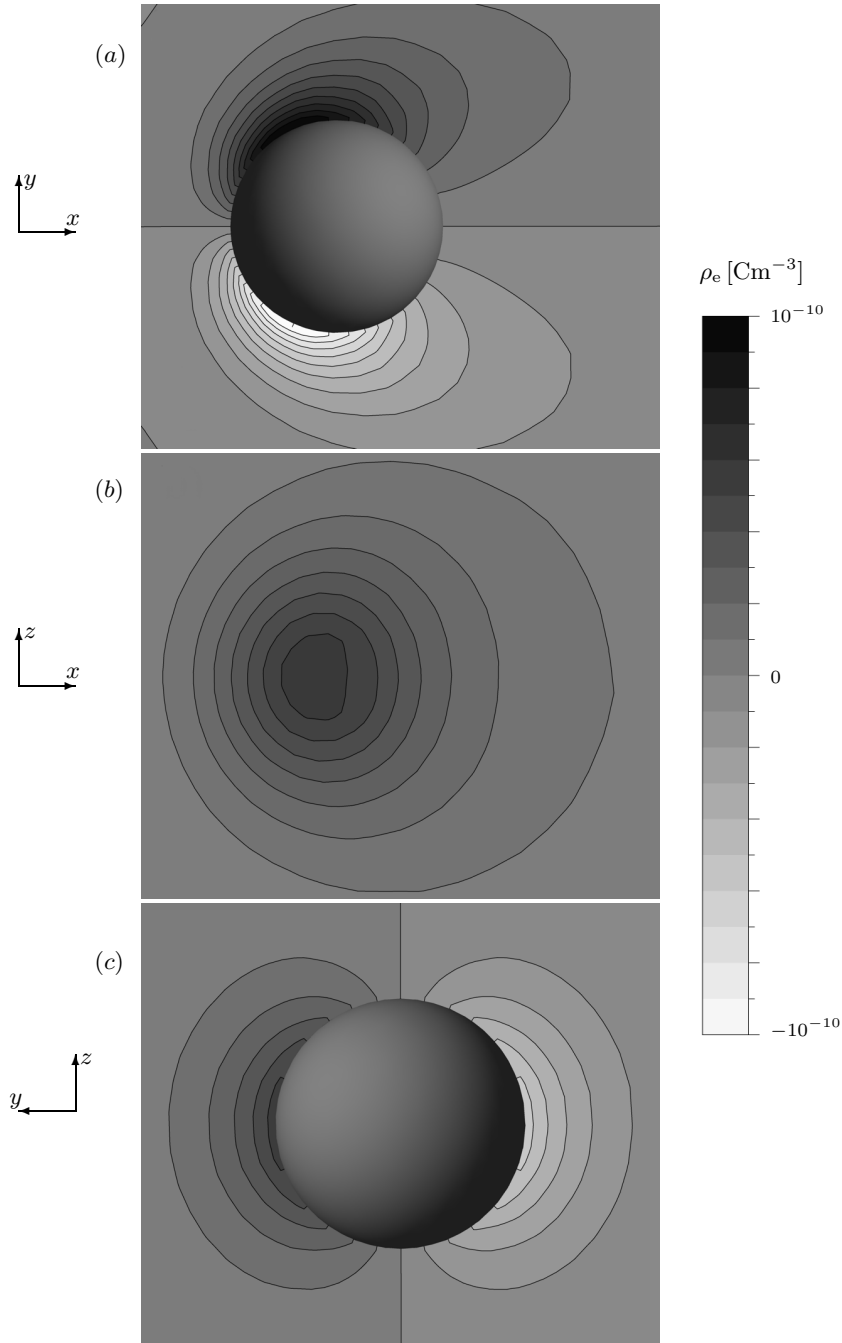

Fig. 6. The volume charge density ρ_e in (*a*) the xy-plane, (*b*) the xz-plane touching the side of the sphere and (*c*) the yz-plane for Re = 10 and Ha = 2.
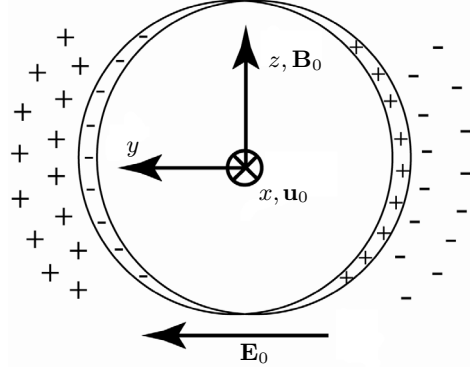
Fig. 7. Schematic drawing of the location and sign of the volume and surface charge arising in the configuration studied.

Note that the total charge involved is very small, typically of the order of a single electron charge. This shows the nature of the charge density as a come and go of electrons. In the resulting steady state distribution the positive nuclei are almost, but not completely, cancelled by free electrons subject to electric and magnetic forces. More quantitatively we can look at a case when $\mathrm{Ha}^2 \ll \mathrm{Re} \ll 1$ so that $\mathrm{N} \ll 1$ and magnetohydrodynamic effects are negligible. In this case, the fluid velocity is given by the Stokes flow solution [17]. In spherical coordinates, with θ being the azimuthal angle with the x-axis and ϕ the polar angle from the y-axis, as shown in Fig. 1, the vorticity is in the ϕ-direction and in magnitude given
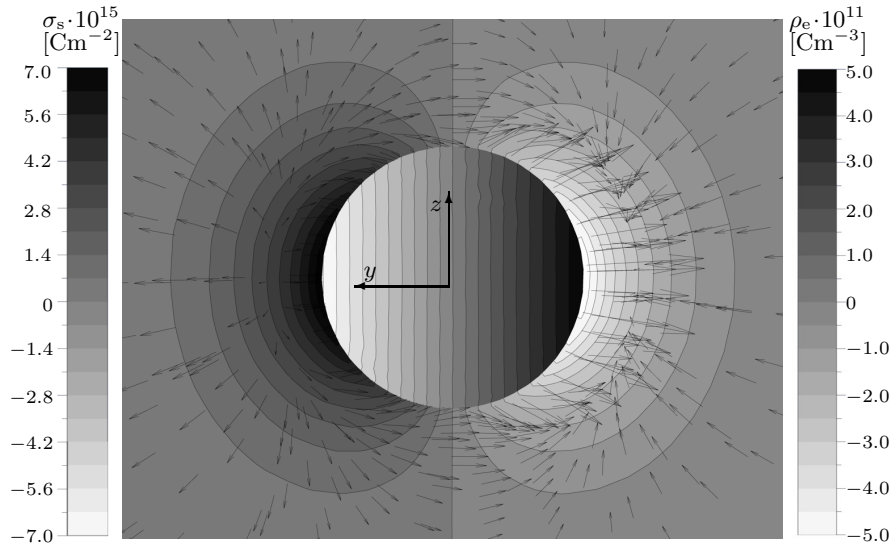

Fig. 8. Contours of the surface charge density σ_s and volume charge density ρ_e for $\mathrm{Re} = 10$ and $\mathrm{Ha} = 2$. The vectors show the electric field produced by these charges, i.e., the total electric field minus the applied electric field $\mathbf{E}_0$. Close to the sphere the normal component of this induced electric field is equal and opposite to that of the applied electric field, owing to the presence of surface charge. At some distance from the sphere, however, the volume charge of opposite sign changes the direction of the induced electric field.

119

by $\omega = -3u_0 a \sin\theta/2r^2$. Eq. 3 with a magnetic field $\mathbf{B}_0$ in the z-direction yields a volumetric charge density $\rho_e = 3E_0 a \sin\theta \cos\phi/2r = 3E_0 ay/2r^2$ with $E_0 = u_0 B_0$. Neglecting this volume charge, the electric potential is given by

$$\Phi(r,\psi) = \begin{cases} E_0 \left(y - r \cos(\psi)/2 \right) & r \leq a \\ E_0 \left(y - a^3 \cos(\psi)/2r^2 \right) & r \geq a, \end{cases} \tag{8}$$

with ψ being the angle with the y-axis as shown in Fig. 1. The electric potential of Eq. 8 satisfies the Laplace equation $\nabla^2\Phi = 0$ together with the appropriate boundary conditions $E_r(r = a, \psi) = 0$ and $\mathbf{E}(r \to \infty, \psi) = \mathbf{E}_0$. From Eq. 7 the surface charge can be evaluated as $\sigma_s(\psi) = -3\epsilon_0 E_0 \cos\psi/2 = -3\epsilon_0 E_0 y/2r$. Note that this expression closely resembles the expression for the volumetric charge density, apart from the characteristic sign difference. In general, however, the volume charge will have a significant impact on the potential distribution. Note that from the expression obtained for ρ_e there is actually an infinite amount of charge on either side of the xz-plane. This is due to the fact that with the $1/r$ behaviour of the velocity and the resulting $1/r^2$ behaviour of the vorticity, the volumetric charge density ρ_e decays quite slow with a distance r from the sphere. For Re $\gg 1$, the velocity decays faster with distance from the sphere so that a finite amount of charge is located in a thin layer of thickness $\mathcal{O}(D/\sqrt{\text{Re}})$ from the sphere. In this case, the potential distribution of Eq. 8 is totally altered by the presence of volume charge, as can be seen in Fig. 9.

4.2. Other regimes. In this section we will investigate three parameter ranges differing from the case Re = 10, Ha = 2 discussed previously. The relative magnitude of the velocity and electric current density are displayed in Fig. 10. Observe, in particular, the various degrees of asymmetry introduced by the magnetic field mainly dictated by N, the thickness of the Hartmann layer mainly dictated by Ha, but evidently also by Re, and the degree of electric current downstream the sphere mainly determined by Re.
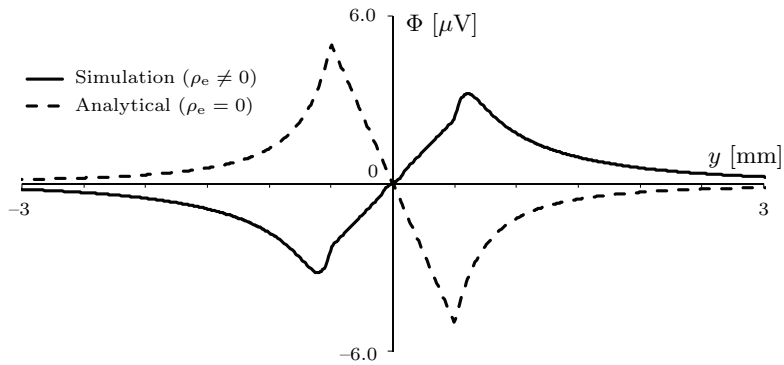

Fig. 9. The electric potential Φ along the y-axis caused by the surface charge and volume charge density ρ_e near the sphere, i.e., the total potential minus the potential $-E_0 y$ of the applied electric field. A sphere diameter of $D = 1$ mm, a main flow velocity of $u_0 = 0.1$ ms^{-1} and a magnetic field of $B_0 = 0.2$ T were used so that Re = 100 and Ha = 2. The data is compared to the analytical electrostatic solution for $\rho_e = 0$ (Eq. 8). The presence of volume charge, however, which is confined to a boundary layer of the order $D/\sqrt{\text{Re}} = D/10$ as can be seen from the figure, totally alters the potential distribution. Only just outside the sphere is the simulated electric field equal to that of the analytical solution as required by the electrostatic boundary condition.
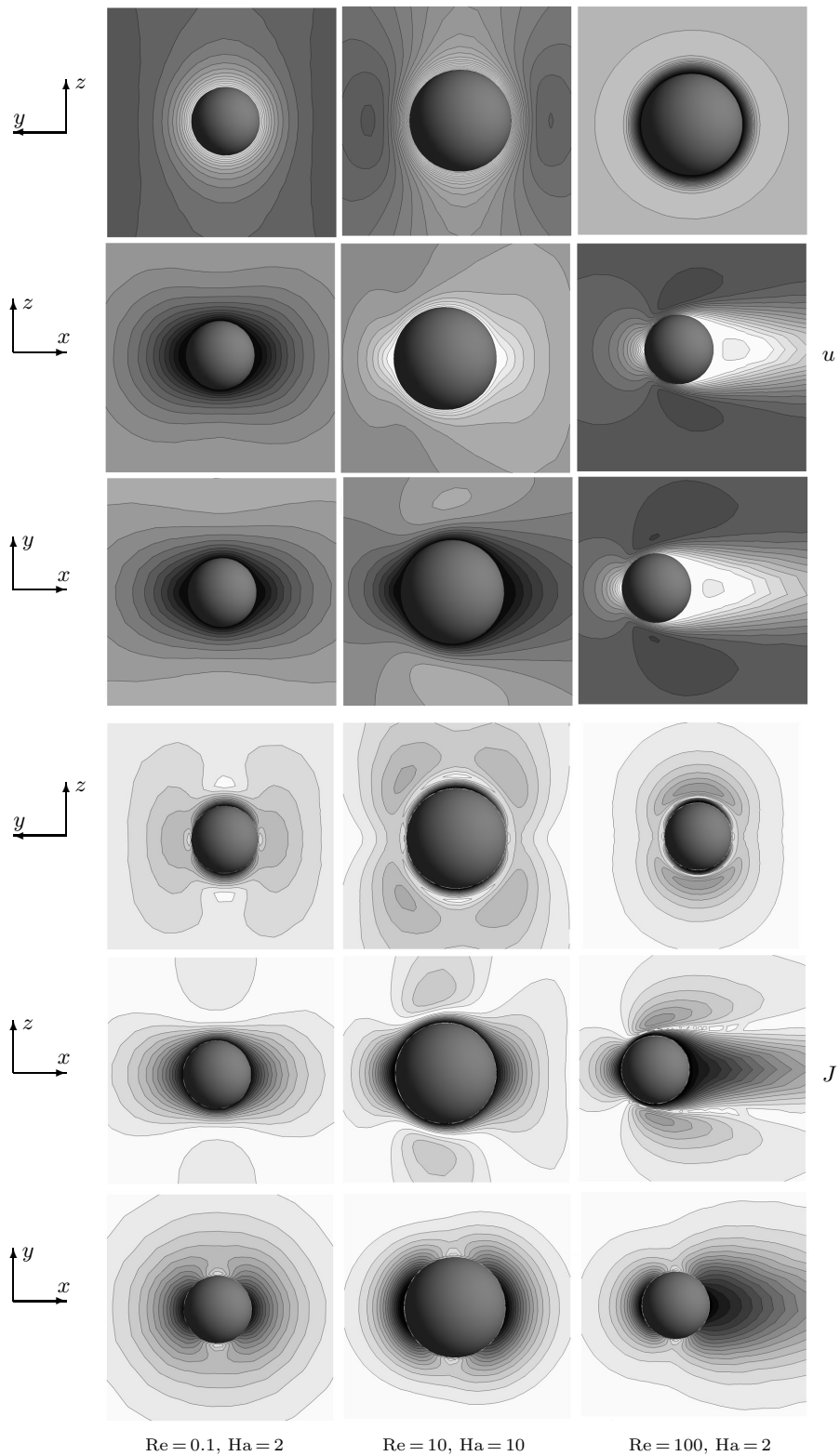
Fig. 10. Contours (top) of the relative magnitude of the velocity and (bottom) of the electric current density.

1. Re = 0.1 and Ha = 2 so that N = 40. The first case can be compared with the hydrodynamic Stokes flow around a sphere, in which inertial effects are negligible so that there is a symmetry between the region upstream and downstream of the sphere. This symmetry can approximately be seen from Fig. 10. Comparing with the long-range $1/r$ behaviour of viscous Stokes flow, it is not surprising that the currents extend to quite some distance from the sphere. A volume charge present, further increases the electric currents near the sides of the sphere. This electric current accelerates the flow, yielding a distinctly asymmetric flow profile, in contrast with the axisymmetric hydrodynamic Stokes flow.

2. Re = 10 and Ha = 10 so that N = 10. The second case approximately satisfies the requirements $Ha^2 \gg Re \gg 1$ set by the theory of Ref.[12], albeit that this specific analytical result assumes that the channel walls are close to the sphere. In this limiting case, Ref. [12] shows that the fluid velocity drops to zero in a column parallel to the magnetic field from the sphere to the walls, This region is patched by a shear layer to the plane potential flow away from the sphere. The beginning of the formation of a region of still liquid, above and below the sphere, can be seen in Fig. 10. The prediction of a Hartmann current layer varying in thickness as the cosine of the angle between the surface normal and the magnetic field can roughly be seen from the figure. Due to a slight numerical instability in this demanding flow regime, the profiles are not entirely symmetric along the y-coordinate.

3. Re = 100 and Ha = 2 so that N = 0.04. The third case has a very small interaction parameter such that the magnetic effects far away from the sphere are negligible. Indeed, a very little difference can be seen between a view parallel and a view perpendicular to the magnetic field. The shape of the current profile closely mimics the velocity profile. Due to the large influence of inertial effects, the current profiles show the largest extent in the streamwise direction of all three cases.

4.3. Electromagnetic drag. Various simulations have been performed to calculate the increase in drag force on the sphere upon application of the magnetic field. In all calculations an electric field $\mathbf{E}_0 = -\mathbf{u}_0 \times \mathbf{B}_0$ has been applied to prevent the formation of electric currents far away from the sphere and to thereby exclude
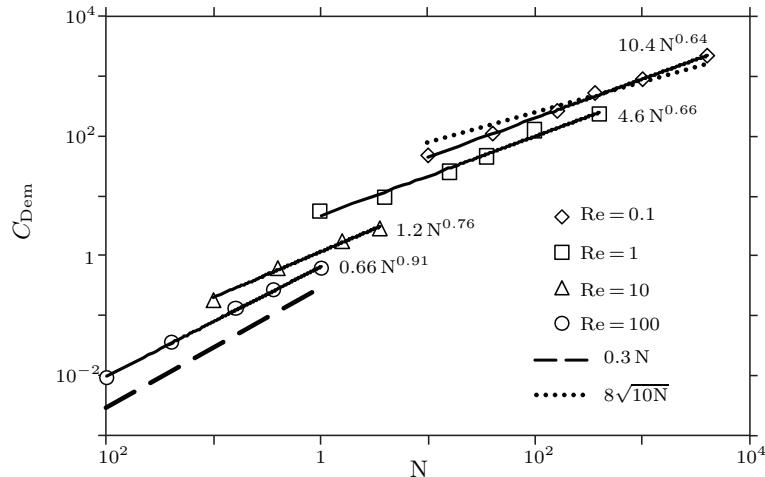

Fig. 11. The results of the simulations for the electromagnetic drag coefficient C_{Dem} together with the theoretical limits $C_{\mathrm{Dem}} = 3N/10$ for $N \ll 1 \ll Re$ [9] and $C_{\mathrm{Dem}} = 8\sqrt{N}/\sqrt{Re}$ for $N, Re \gg 1$ [13], here displayed for Re = 0.1.

Table 1. The drag coefficients C_{D0} resulting from simulations without an applied magnetic field are compared with the the correlations given by Ref. [18].

Re	C_{D0} (sim.)	C_{D0} [18]
0.1	272	244
2	15.4	14.8
10	4.43	4.26
100	1.20	1.09

the effect of the electromagnetic Archimedes force [5]. A somewhat coarser mesh, compare to the one used for the simulations discussed previously, was used to make the computational time tractable. Simulations without an applied magnetic field have been compared with various correlations from Ref. [18] in Table 1. The results show an overestimation of the simulated drag force up to approximately 10%. A similar accuracy was found by extrapolating the mesh dependence of the drag force and was considered satisfactory for present purposes. The simulations were performed in the range $0.1 \leq \text{Re} \leq 100$ and $1 \leq \text{Ha} \leq 20$ covering the interaction parameters ranging from 10^{-2} to $4 \cdot 10^3$. An overview of the results is shown in Fig. 11. The wide range of interaction parameters makes comparison with earlier results possible:

• For interaction parameters $N \geq 10$ the results agree to within thirty percent with the analytical result $C_{\text{Dem}} = 8\sqrt{N}/\sqrt{\text{Re}}$ of Eq. 5. This approximate correspondence is slightly surprising because the requirements set by the corresponding theory of Ref. [12] include a high Reynolds number and the sphere diameter being of the same order of magnitude as the channel height. In our simulations we have some correspondence for fairly low Reynolds numbers and no walls near the sphere.

• At the bottom left of Fig. 11, the drag coefficient approaches the theoretical potential theory limit $C_{\text{Dem}} = \frac{3}{10}N$ [9] valid for $\text{Re} \gg 1$ and $N \ll 1$.

From the results in Fig. 11 it follows that C_{Dem} can locally be quite well parameterized by a power function of the interaction parameter N:
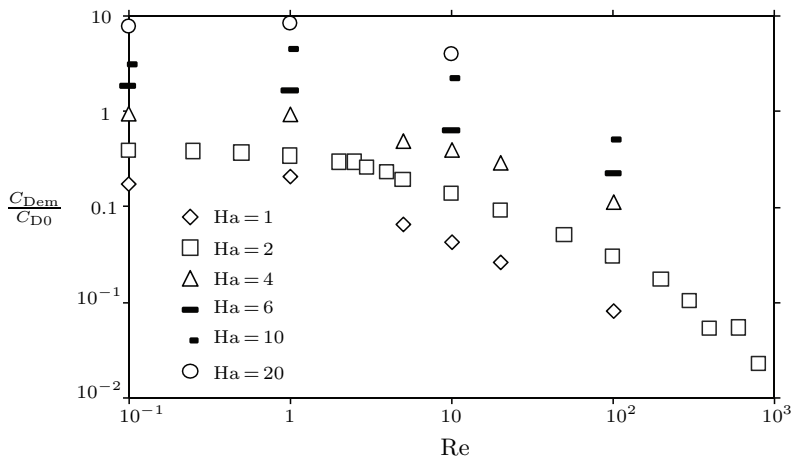
$$C_{\text{Dem}} = f(\text{Re}) \cdot N^p. \tag{9}$$

Fig. 12. The relative electromagnetic drag C_{Dem}/C_{D0} becomes independent of Re for low values of Re consistent with the analytical solution for magnetohydrodynamic Stokes flow [8].
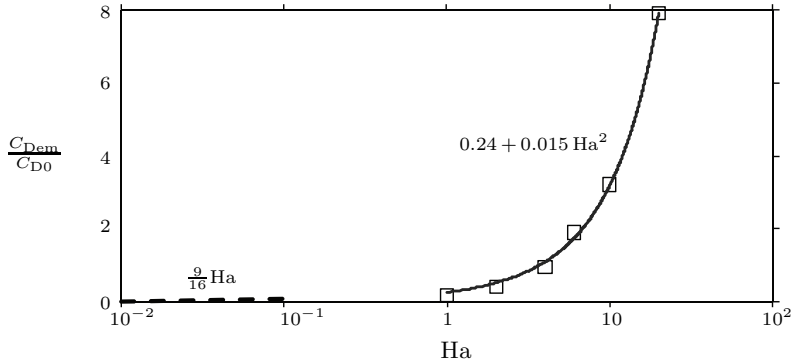
Fig. 13. The analytical result for the relative electromagnetic drag $C_{\text{Dem}}/C_{\text{D0}}$ for Ha, Re $\ll 1$ [8] is extended with simulations to $1 \leq \text{Ha} \leq 20$.

In accordance with the theoretical result of [13], the coefficient f is a function of Re. It must, however, be noted that because C_{Dem} is proportional to N for N $\ll 1$ (Eq. 4) and proportional to $\sqrt{\text{N}}$ for N $\gg 1$ (Eq. 5), the exponent p has to be a function of N as well. The parameterization of Eq. 9 is thus strictly valid only as a limiting description for either N $\gg 1$ or N $\ll 1$. For N $\gg 1$, for which we have the most significant change in the drag coefficient, fortunately there is agreement between the two existing analytical limits for Re $\ll 1$ and Re $\gg 1$ about the functional form of the drag. Both the result of Eq. 6 for Re $\ll 1$ and the result of Eq. 5 for Re $\gg 1$ have the same $\sqrt{\text{N}}/\sqrt{\text{Re}} = \text{Ha}/\text{Re}$ dependence and are of similar magnitude. For the log-log plot of Fig. 11 the parameterization of Eq. 9 yields $\log C_{\text{Dem}} = \log f(\text{Re}) + p \log \text{N}$ so that for N $\gg 1$ (N > Re for low Re, the curves for constant Re will tend to a slope $p = 1/2$ and will have a vertical shift proportionally to $\log 1/\sqrt{\text{Re}} = -(\log \text{Re})/2$. For N $\ll 1$ the high Re curves all will collapse at some point onto the gray dashed line 0.3N at the bottom left.

From Fig. 12 it can be seen that for Re $\ll 1$ the ratio $C_{\text{Dem}}/C_{\text{D0}}$ becomes more or less independent of Re, in agreement with Eq. 6, which was derived as a polynomial in Ha [8] and only holds for Ha $\ll 1$. As an extension of this analytical solution to $1 \leq \text{Ha} \leq 20$, our results can be fitted as a power series in Ha, as depicted in Fig. 13:

$$C_{\text{Dem}} = \left(0.24\text{Ha} + 0.015\text{Ha}^2\right) C_{\text{D0}} \qquad 1 \leq \text{Ha} \leq 20, \text{Re} \ll 1.$$

5. Conclusions. A rich physical structure has been revealed for the magnetohydrodynamic flow around an insulating sphere with crossed electric and magnetic fields perpendicular to the main flow. The interplay between the flow and the electromagnetic fields dictates the formation of oppositely charged volume and surface charges on the sides of the sphere. The presence of these volume charges was found to play a role in the dynamics of the electric current density and was thereby found to significantly influence the velocity profiles. The results from our simulations on the electromagnetic drag approach various theoretical limits and show that the electromagnetic drag coefficient can locally effectively be parameterized as a power of the interaction parameter with coefficient and exponent decreasing and increasing with the Reynolds number, respectively. The obtained results apply to spherical objects in a conducting fluid, moving perpendicular to a magnetic field as well as to duct flows in the presence of a magnetic field perpen-

dicular to the main flow, making them useful for various magnetohydrodynamic applications with insulating inclusions.

REFERENCES

[1] P. DAVIDSON. *An Introduction to Magnetohydrodynamics* (Cambridge University Press, 2001).

[2] B. LI. Solidification processing of materials in magnetic fields. *JOM-e*, vol. 50 (1998), no. 2.

[3] E. TZIRTZILAKIS. A mathematical model for blood flow in magnetic field. *Phys. Fluids*, vol. 17 (2005).

[4] S. QIAN AND H. BAU. Magneto-hydrodynamics based microfluidics. *Mech. Res. Comm.*, vol. 36 (2008), pp. 10–21.

[5] D. LEENOV AND A. KOLIN. Theory of electromagnetophoresis. i. magnetohydrodynamic forces experienced by spherical and symmetrically oriented cylindrical particles. *J. Chem. Phys.*, vol. 22 (1953), pp. 683–688.

[6] V. BAZILEVSKII *et al.* Mhd separation of molten salt slags in alminum smelting. *Magnetohydrodynamics*, vol. 6 (1970), no. 2, pp. 157–159.

[7] W. CHESTER. The effect of a magnetic field on stokes flow in a conducting fluid. *J. Fluid Mech.*, vol. 3 (1957), pp. 304–308.

[8] K. GOTOH. Stokes flow of an electrically conducting fluid in a uniform magnetic field. *J. Phys. Soc. Jpn*, vol. 15 (1960), pp. 696–705.

[9] J. REITZ AND L. FOLDY. The force on a sphere moving through a conducting fluid in the presence of a magnetic field. *J. Fluid Mech.*, vol. 11 (1961), pp. 133–142.

[10] K. KALIS, N. SLYUSAREV, A. TSINOBER, A. SHTERN. Resistance of bluff bodies at high stewart numbers. *Magnetohydrodynamics*, vol. 2 (1966), no. 4, pp. 152–153.

[11] G. BRANOVER, N. SLYUSAREV, A. TSINOBER. Drag of a sphere in a magnetohydrodynamic flow. *Magnetohydrodynamics*, vol. 2 (1966), no. 3, pp. 149–150.

[12] J. HUNT AND G. LUDFORD. Three-dimensional MHD duct flows with strong transverse magnetic fields. Part 1. Obstacles in a constant area channel. *J. Fluid Mech.*, vol. 33 (1968), pp. 693–714.

[13] J. HUNT. Bluff body drag in a strong transverse magnetic field. *Magnetohydrodynamics*, vol. 6 (1970), no. 1, pp. 35–38.

[14] T. SEKHAR, R. SIVAKUMAR, AND T. RAVIKUMAR. Magnetohydrodynamic flow around a sphere. *Fluid Dyn. Res.*, vol. 37 (2005), pp. 357–373.

[15] T. SEKHAR, T. RAVIKUMAR, AND H. KUMAR. Mhd flow past a sphere at low and moderate reynolds numbers. *Comp. Mech.*, vol. 31 (2003), pp. 437–444.

[16] R. MOREAU. *Magnetohydrodynamics* (Springer, 1990).

[17] G. BATCHELOR. *An introduction to fluid dynamics* (Cambridge University Press, 1967).

[18] J. GRACE, R. CLIFT, AND M. WEBER. *Bubbles Drops and Particles* (Academic Press, Inc., 1978).